Earth and Planetary Science Letters 282 (2009) 24–33

Contents lists available at ScienceDirect

Earth and Planetary Science Letters

journal homepage: www.elsevier.com/locate/epsl

Polarity reversals in geodynamo models with core evolution

Peter Driscoll *, Peter Olson

Department of Earth and Planetary Sciences, Johns Hopkins University, Baltimore, MD 21218, USA

ARTICLE INFO

Article history:
Received 18 November 2008
Received in revised form 13 February 2009
Accepted 16 February 2009
Available online 18 March 2009

Editor: T. Spohn

Keywords:
numerical dynamos
geodynamo
polarity reversals
magnetic superchrons
core thermal history
tidal deceleration

ABSTRACT

Numerical dynamos with time-variable control parameters that simulate the secular evolution of the core are used to interpret long-term trends in geomagnetic field behavior, including polarity reversal frequency. Dynamos with incremental changes in convective forcing and rotation rate show continuous trends in dipole field intensity and fluid velocity, with systematic variations in polarity chrons in some cases. Otherwise similar dynamos with constant forcing and rotation rate have statistically stationary dipole field intensity and fluid velocity, with random polarity chrons. A reversing dynamo with steady rotational deceleration constrained by tidal friction and a decreasing (regular) inner core growth rate constrained by core thermal history evolves over 10 Myr with minor trends in average dipole intensity, fluid velocity, and polarity chron length. In contrast, a dynamo started in a non-reversing state and subject to an increasing (anomalous) inner core growth rate and constant rotation evolves over 20 Myr to a reversing state with substantial trends in dipole intensity and polarity chron length. The dispersion of polarity chron lengths in the dynamo model with anomalous evolution is qualitatively similar to the observed dispersion of geomagnetic polarity chrons since the end of the Cretaceous Normal Superchron, and the model dipole field frequency spectra are qualitatively similar to estimates of the geomagnetic spectrum at very low frequencies.

1. Introduction

The geomagnetic field is maintained by dynamo action in the Earth's core. Because the dynamo process in the core requires energy sources and is influenced by planetary rotation, changes in the energetics of the core and variations in the rate of planetary rotation over time are expected to have observable consequences for the geomagnetic field. Two properties of the geomagnetic field in particular may be sensitive to these controls: the time-averaged dipole field intensity and the frequency of polarity reversals. Paleomagnetic intensity data present a mixed picture in regard to long-term geomagnetic dipole variations. There is little evidence for a trend in the dipole intensity over the Phanerozoic, although there is some evidence for higher intensity fields at a few specific times, such as during the Cretaceous Normal Superchron, or CNS (Heller et al., 2002; Valet, 2003; Tauxe and Yamazaki, 2007). In contrast, there are clear indications that the average frequency of polarity reversals has changed over time, with evidence for three superchrons in the Phanerozoic (Pavlov and Gallet, 2005) and the well-documented trend of increasing frequency of reversals from the end of the CNS to the present (Gallet and Courtillot, 1995; Constable, 2000, 2003).

Long-term trends in reversal frequency and the 100–200 Myr spacing of superchrons suggests an influence of the mantle on the core (Merrill and McFadden, 1999; Courtillot and Olson, 2007), but several modeling studies have shown that purely stochastic fluctuations of reversal frequency can explain the occasional superchron (Hoyng et al., 2001; Hulot and Gallet, 2003; Jonkers, 2003; Ryan and Sarson, 2007), without the need for time-variable mantle control or core evolution. In light of these competing interpretations, it is important to determine how the geodynamo responds to various styles of core evolution in order to distinguish evolutionary changes from stochastic fluctuations in the paleomagnetic record.

The simplest way to estimate the sensitivity of the geodynamo to core evolution is to compare numerical dynamo models that represent discrete stages in the evolution of the core. This approach has been used to determine the geomagnetic field sensitivity to changes in the size of the inner core (Sakuraba and Kono, 1999; Roberts and Glatzmaier, 2001; Heimpel et al., 2005). It has also been used to estimate the geodynamo sensitivity to simultaneous changes in convection and rotation (Roberts and Glatzmaier, 2001; Driscoll and Olson, 2007). The stage approach implicitly assumes there is a large separation of the underlying time scales, specifically, that the dynamical time scales of the geodynamo are much shorter than the time scales that characterize core evolution and mantle convection. There are indications that this assumption may not always be justified. Observationally, the geomagnetic dipole frequency spectrum shows increasing variance with decreasing frequency (Courtillot and Le Moul, 1988) with peak variance at frequencies less than 0.1 Myr^{-1} (Constable and Johnson, 2005). Theoretically, it has been shown that some numerical dynamos contain their largest variability at comparably low frequencies (Olson, 2007).

In this paper we compare trends in magnetic field intensity, convective velocity, and polarity reversal behavior over 10–20 Myr time intervals in numerical dynamos that incorporate core evolution in the form of time-dependent control parameters. We show that a transition

* Corresponding author. Fax: +1 410 516 7707x7933.
E-mail address: peter.driscoll@jhu.edu (P. Driscoll).

0012-821X/$ – see front matter © 2009 Elsevier B.V. All rights reserved.
doi:10.1016/j.epsl.2009.02.017

from a superchron to a reversing state with progressively shorter polarity chrons and weaker dipole field occurs as the total convective forcing is increased, a condition we call anomalous dynamo evolution. Regular dynamo evolution, in which the changes in total convective forcing are constrained by core thermal history and the changes in rotation rate are constrained by tidal friction, shows less evolution in dipole intensity and reversal rate, because the dynamical effects of simultaneous decreases in rotation rate and convective forcing tend to balance.

2. Geodynamo evolution model

Consider the slow evolution of the core, beginning at an arbitrary starting time t_s and continuing to some arbitrary ending time t_e. During the time interval $\Delta t = t_e - t_s$ we assume the inner core radius r_i, the volume-averaged light element concentration in the outer core χ_o, and the planetary rotation rate Ω all vary by small amounts. Other core properties will also change during this time interval, such as the mean core temperature, radioactive heat content, electrical conductivity as well as other transport properties, and core-mantle boundary heat flow, but in this study we restrict our analysis to small changes in r_i, χ_o, and Ω.

These variations imply time dependence for several of the geodynamo control parameters. For simplicity, our numerical evolution model considers a linear time variation in those control parameters. To first order, the evolution of the Ekman number E, the ratio of viscous to Coriolis forces, can be written for this interval of time as

$$E \equiv \frac{\nu}{\Omega D^2} = E_s + (t - t_s)\dot{E} \tag{1}$$

where ν is fluid kinematic viscosity and $D = r_o - r_i$ is the outer core shell thickness (r_o being the outer core radius). Here E_s is the starting Ekman number and $\dot{E}$ is its rate of change. Similarly, the evolution of the Rayleigh number Ra, which measures the ratio of buoyancy to viscous forces, can be written for compositional convection over the same time interval as (Jones, 2007; Olson et al., 2009)

$$\mathrm{Ra} \equiv \frac{\beta g_o D^5 \dot{\chi}_o}{\nu^2 \kappa} = \mathrm{Ra}_s + (t - t_s)\dot{\mathrm{Ra}} \tag{2}$$

where κ is the light element diffusivity, g_o is gravity at radius r_o, $\beta = -(\partial\rho/\partial\chi)/\rho$, and ρ is outer core mean density. The coefficients of the assumed linear time variation in (1) and (2) can be written in terms of r_i, Ω, and χ_o and their time derivatives as

$$\dot{E} = \left(\frac{2\dot{r}_i}{D} - \frac{\dot{\Omega}}{\Omega}\right) E_s \tag{3}$$

and

$$\dot{\mathrm{Ra}} = \left(\frac{\ddot{\chi}_o}{\dot{\chi}_o} - \frac{5\dot{r}_i}{D}\right) \mathrm{Ra}_s \tag{4}$$

where we have used $\dot{D} = -\dot{r}_i$.

Expressions for $\dot{r}_i$, $\dot{\chi}_o$, and $\ddot{\chi}_o$ are found by taking time derivatives of thermal history models for the core that link the growth of the inner core to the change in light element concentration of the outer core (Buffett, 2003). As these models are generally not linear, we adopt a power-law representation of the growth of the inner core. Denoting the age of the inner core by τ, and assuming that $t = 0$ corresponds to the time of inner core nucleation, the growth of the inner core due to secular cooling can be approximated by a power-law in time of the form

$$\frac{r_i(t)}{r_i(\tau)} = \left(\frac{t}{\tau}\right)^{2/3} \tag{5}$$

where the 2/3-power has been chosen to approximate the inner core growth history predicted by more complex core evolution models (Gubbins et al., 2003; Labrosse, 2003; Nimmo et al., 2004; Butler et al., 2005; Nimmo, 2007). The rate of change of outer core light element concentration is directly proportional to the rate of inner core growth. Assuming complete partitioning of light elements into the outer core, this relationship is (Loper, 2007)

$$\dot{\chi}_o = \frac{3\chi_o}{(1 - \beta\chi_o)} \frac{r_i^2 \dot{r}_i}{(r_o^3 - r_i^3)} \tag{6}$$

Table 1 gives the estimates of E and Ra determined from the present-day structure of the core and from considerations of its present-day energetics. Changes in these parameters, specifically $\dot{E}$ and $\dot{\mathrm{Ra}}$, are less well-constrained, but they can be crudely estimated from the rotational history of the Earth and models of the thermo-chemical evolution of the core.

Suppose we set $t_e = \tau$ and $(t_e - t_s) = 100$ Myr, so that the starting time t_s corresponds to the middle of the CNS and the ending time is the present-day. Over this time interval there have been large changes in polarity reversal frequency (0–4 Myr^{-1}), but only modest changes in rotation rate, outer core composition, and inner core size. Table 1 gives an estimate for $\dot{\Omega}$ assuming a linear decrease in rotation rate, according to calculations of present-day and recent past tidal friction (Lambeck, 1980; Stacy, 1992), plus fossil evidence from Cenozoic and Paleozoic marine invertebrates (Zharkov et al., 1996; Zhenyu et al., 2007). Assuming a nominal inner core age of $\tau = 1$ Ga, (5) gives the inner core growth rates and (6) gives the outer core light element enrichment rates shown in Table 1.

Differences between the present-day and 100 Ma values are denoted in Table 1 by the prefix Δ. To calculate the change in E and Ra from (1) and (2), respectively, the derivatives are evaluated at the present-day. As anticipated from the slow rate of core evolution, the fractional change in each parameter is rather small: $\Delta E/E \simeq +8\%$, $\Delta\mathrm{Ra}/\mathrm{Ra} \simeq -7\%$, and $\Delta r_i/r_i \simeq +7\%$, respectively. Properties of the geodynamo that are only weakly dependent on the values of E, Ra, and r_i are therefore not expected to change significantly in response to such a small amount of core evolution. However, if the geodynamo lies close to a regime boundary in some of its properties, then even this

Table 1
Core evolution parameters.

Parameter	Value	Units	Source
r_i	1221	km	Dziewonski and Anderson (1981)
$\dot{r}_i$	814	km Gyr^{-1}	Eq. (5)
$\ddot{r}_i$	−271	km Gyr^{-2}	Eq. (5)
χ_o	0.1	–	Wood et al. (2006)
$\dot{\chi}_o$	0.01	Gyr^{-1}	Eq. (6)
$\ddot{\chi}_o$	0.01	Gyr^{-2}	Eq. (6)
g_o	10.68	m s^{-2}	Dziewonski and Anderson (1981)
D	2259	km	Dziewonski and Anderson (1981)
r_c	3480	km	Dziewonski and Anderson (1981)
ν	1.26×10^{-6}	$\mathrm{m}^2\ \mathrm{s}^{-1}$	Terasaki et al. (2006)
κ	10^{-8}	$\mathrm{m}^2\ \mathrm{s}^{-1}$	Gubbins et al. (2004)
η	2	$\mathrm{m}^2\ \mathrm{s}^{-1}$	Jones (2007)
t_d	20	kyr	Eq. (7)
β	1	–	Jones (2007)
Ω	7.29×10^{-5}	rad s^{-1}	Stacy (1992)
$\dot{\Omega}$	-2.22×10^{-22}	rad s^{-2}	Zharkov et al. (1996)
E	3×10^{-15}	–	Eq. (1)
Ra	1×10^{34}	–	Eq. (2)
Pr	126	–	–
Pm	6×10^{-7}	–	–
Δt	5000	t_d	–
Δr_i	83	km	–
$\Delta\chi_o$	9.44×10^{-4}	–	–
$\Delta\Omega$	-7.00×10^{-7}	rad s^{-1}	–
$\Delta E/E$	0.082	–	Eq. (3)
$\Delta\mathrm{Ra}/\mathrm{Ra}$	−0.071	–	Eq. (4)

Parameter values correspond to the present-day core. Differences between present-day and 100 Ma are denoted by Δ.

small amount of core evolution could produce a large change in those properties. For example, numerical dynamo modeling (Kutzner and Christensen, 2002; Driscoll and Olson, 2007) and reversing dynamo experiments (Berhanu et al., 2007) have shown that the transition from frequent to non-reversing behavior typically occurs within a very narrow slice of parameter space. If the geodynamo lies within such a narrow slice, then a small amount of core evolution may result in greatly magnified changes in geomagnetic polarity reversal behavior.

3. Evolving numerical dynamos

In order to simplify the comparison of evolving and fixed parameter dynamo models, we limit our consideration to dynamos driven by chemical convection (no thermal buoyancy included) modeled by a constant sink term in the light element transport equation (Kutzner and Christensen, 2000), which is the dimensionless measure of the rate of light element enrichment in the outer core. We fix the Prandtl number, ratio of viscous to compositional diffusivity, to $\mathrm{Pr}=1$ and the magnetic Prandtl number, ratio of viscous to magnetic diffusivity, to $\mathrm{Pm}=20$ in all cases. We use identical sets of boundary conditions in all cases: no-slip and electrically insulating at r_i and r_o, fixed light element concentration at r_i and zero light element flux at r_o. We use the dynamo code *mag* available at *www.geodynamics.org*.

Dynamo evolution involves long simulation times, which necessitate a relatively sparse grid and large time steps. Here we use the same numerical grid for all the calculations, with spherical harmonic truncation at $l_{max}=32$ and average radial resolution of 88 km. This restricts us to relatively large Ekman numbers, $5\text{–}6.5\times10^{-3}$. The advantages and disadvantages of large Ekman numbers in modeling the geodynamo are described by Wicht (2005), Christensen and Wicht (2007), Aubert et al. (2008), and Olson et al. (2009), but the compelling factor in our study is the need to extend the simulation time as far as possible. The current threshold Ekman number in geodynamo modeling is around 10^{-6}–10^{-7} (Takahashi et al., 2008; Kageyama et al., 2008) and polarity reversals have been found in low E dynamos (see Glatzmaier and Coe, 2007; Takahashi et al., 2007). Unfortunately, low E dynamos require too much spatial and temporal resolution to simulate multi-million year time intervals. Dynamo simulations covering substantial intervals of geologic time have traditionally been considered impractical, but recently Wicht et al. (2009) report a 160 Myr simulation that produces several hundred polarity reversals, using fixed (i.e., non-evolving) values of the control parameters that are roughly comparable to the time-average parameters in our study.

An additional consideration is whether these models are in the correct energetic regime, specifically, whether the ratio of magnetic and kinetic energies in the model is comparable to that of the geodynamo. Near the CMB, using typical values of the geomagnetic field strength ($\approx$0.4 mT) and fluid velocity ($\approx$1 mm s^{-1}), the ratio of magnetic to kinetic energy is ~ 13. This is somewhat larger than the volume-averaged ratio in our model of ~ 3. The fact that our model energy ratio exceeds one is due in part to our choice of a large Pm, which partially compensates for our choice of large Ekman number. However, this ratio is expected to be even larger in the core interior, because the geomagnetic field is expected to amplify with depth faster than the fluid velocity.

The parameters of four dynamo models are given in Table 2. Two of these cases include parameter evolution, while the other two are fixed parameter cases for comparison. Case R is intended to model the regular evolution of the core. It assumes that the ratio of $\Delta E/E$ to $\Delta\mathrm{Ra}/\mathrm{Ra}$ is ~1, approximately the same ratio predicted for monotonic power-law cooling of the core and steady tidal deceleration according to the data in Table 1. The evolution of case R is considered to be regular because the direction of evolution in Ra–E space is approximately the same as the secular evolution of the core over the last 100 Myr, however the rate of evolution in the model is faster than in the Earth, as described below. The corresponding fixed parameter case is denoted by R^*. Cases R and R^* are started from similar E_s and Ra_s values, selected to yield chaotic reversing dynamo behavior as the initial state. Case A represents anomalous evolution of the core, in which $\Delta\mathrm{Ra}/\mathrm{Ra}$ is large and positive, and ΔE is zero. This case is intended to model rapid inner core growth with negligible change in the rotation rate. Rapid inner core growth could result from an episode of enhanced heat loss from the core due to increased vigor of mantle convection, plume formation at D", or the arrival of cold slabs at the core mantle boundary (Hulot and Gallet, 2003). Case A was initialized at relatively low Ra_s, so as to begin in a non-reversing (superchron) state. The corresponding fixed parameter case, denoted by A^*, has a larger Ra and lies in the reversing regime, about 3/4 of the way along the evolutionary trajectory of case A.

Table 2
Dynamo model dimensionless parameters and results.

Dynamo Case	R	R*	A	A*
Evolution Type	Regular	Fixed	Anomalous	Fixed
Δt	500	500	1000	270
Ra_s	3.87×10^4	3.94×10^4	1.69×10^4	2.8×10^4
$\Delta\mathrm{Ra}$	-0.37×10^4	0	$+1.31\times10^4$	0
E_s	5.1×10^{-3}	5.0×10^{-3}	6.5×10^{-3}	6.5×10^{-3}
ΔE	$+0.53\times10^{-3}$	0	0	0
N_{step}	5	0	20	0
B_{rms}	4.59 ± 0.73	4.71 ± 0.72	3.93 ± 0.68	4.03 ± 0.73
ΔB_{rms}	−0.26	0.16	0.20	−0.20
u_{rms}	172.1 ± 17.7	174.4 ± 15.4	137.2 ± 23.7	155.2 ± 12.6
Δu_{rms}	−4.22	−2.11	70	2.34
B_d	0.66 ± 0.21	0.70 ± 0.20	0.61 ± 0.25	0.53 ± 0.21
ΔB_d	−0.09	0.04	−0.35	−0.02
N_{chron}	8	8	26	7
N_{eq}	14	18	66	15
N_{rev}	7	7	25	6
t^{ave}_{chron}	62	55	35	36
Δt_{chron}	30	40	−550(−80)	0
b	−0.64	−0.002	−0.52(−0.03)	−0.60
d	0.51	0.50	0.52(0.47)	0.48

Times are in units of dipole free decay times. Δt is the length of the simulation in dipole decay times, Δ denotes the difference between the final and initial values, N_{step} is the number of steps in parameter evolution, N_{chron} is the number of stable polarity chrons, N_{eq} is the total number of dipole tilt equator crossings, N_{rev} is the total number of dipole polarity reversals, and t^{ave}_{chron} is the average chron length. The polarity bias $b=\bar{p}/\overline{|p|}$ is the ratio of the mean polarity to its rms value, where the polarity function $p=\pm1$ depending on the sign of the axial dipole. Dipolarity d is the ratio of rms dipole B_d to rms total field B on the outer boundary. Means and standard deviations ($\pm$) are given for B_{rms}, u_{rms}, and B_d. Results from the second half of case A are shown in parentheses.

It is convenient to describe the variability in these dynamo models in non-dimensional time units using t_d, the free decay time of a dipole field in a uniformly conducting sphere with radius r_o:

$$t_d=\frac{\mu_0\sigma r_o^2}{\pi^2} \tag{7}$$

where μ_0 is magnetic permeability and σ is electrical conductivity. For the Earth's core, $t_d\approx20$ kyr. Throughout the rest of this paper, dynamo model times are expressed as multiples of t_d (dipole decay units). Likewise, dynamo model fluid velocities are scaled by η/D (magnetic Reynolds number units) and dynamo model magnetic fields are scaled by $\sqrt{\rho\Omega/\sigma}$ (Elsasser number units).

To implement the parameter evolution we use a step system, in which small incremental changes to Ra and E are applied to the models at N_{step} successive times during the run, as given in Table 2. The control parameters are kept fixed between these steps. For each model there is an initial transient period that is discarded, typically a few viscous times which is about 1% of the length of a parameter step. The rest of the time series is continuous, with nothing excluded after each step in the control parameters. Cases R and R^* were run for $\Delta t=500$ dipole decay times, which corresponds to approximately 10 Myr of paleomagnetic time. Cases A and A^* were run for $\Delta t=1000$ and $\Delta t=270$ dipole decay times, respectively, which corresponds to approximately 20 Myr and 5 Myr of paleomagnetic time, respectively.

The rate of evolution in case R is faster than the nominal evolution rate of the core by a factor of 13, and in case A by a factor of 50. Accelerated evolution is necessary in these models because of the cost to make multiple runs of several 100 Myr in length.

In addition to representing continuous parameter changes in discrete steps, these models ignore several other effects that might be important in geodynamo evolution on 100 Myr time scales. All four cases ignore explicit variations in the shell geometry factor $\Delta r_i/r_i$. We justify this simplification based on some model tests with slightly different shell ratio factors, which showed little sensitivity to the minor variations in this parameter that accompany the amounts of core evolution we consider here. In addition, as mentioned previously, thermal buoyancy is ignored in all cases, including changes in the total heat flow from the core and changes in the spatial distribution of heat flow on the core-mantle boundary (Glatzmaier et al., 1999). These effects should rightly be included in a full model of geodynamo evolution although they introduce additional control parameters, requiring still more calculations. Accordingly, we consider these effects beyond the scope of the present study and topics for future work (see Section 5).

4. Results

4.1. Time series

Figs. 1–3 compare time series of rms dipole field intensity B_d on the core boundary in Elsasser number units, rms fluid velocity u_{rms} in magnetic Reynolds number units, and dipole tilt angle in degrees, from cases R, R^*, and A, representing regular, fixed, and anomalous core evolution, respectively. Cases R and R^* are shown for $\Delta t = 500$ dipole decay times whereas case A is shown for $\Delta t = 1000$, split into two equal panels (c) and (d), each of length 500. Case R reaches the parameter changes expected for 100 Myr of core evolution after 400 dipole decay times. Reverse and normal polarity chrons are indicated by white and gray backgrounds, respectively, in each figure. Statistics of each case are given in Table 2 along with the statistics of non-evolving case A^*, which is not shown in Figs. 1–3 because its time series behavior is similar to R^*.

These dynamos are comparable in terms of their overall magnetic field structure. All four are strongly dipolar, with average dipolarities near 0.5. All show low frequency fluctuations in which u_{rms} and B_d are almost exactly one half cycle out of phase, plus higher frequency fluctuations. At low frequencies the correlation coefficient between the magnetic and kinetic energy fluctuations is about -0.95, whereas the phase relationship in the higher frequency fluctuations is time variable and depends on the phase of the low frequency variations. When the low frequency component of B_d is increasing, the high frequency component of u_{rms} leads the high frequency component of B_d by about one quarter cycle. When the low frequency componentof B_d is decreasing, the phase relationship between the high frequency components of u_{rms} and B_d is incoherent.

The four models show multiple dipole collapse events, in which the dipole field falls to a small fraction of its time average intensity $\overline{B}_d$. Some of these collapse events result in dipole axis excursions; others

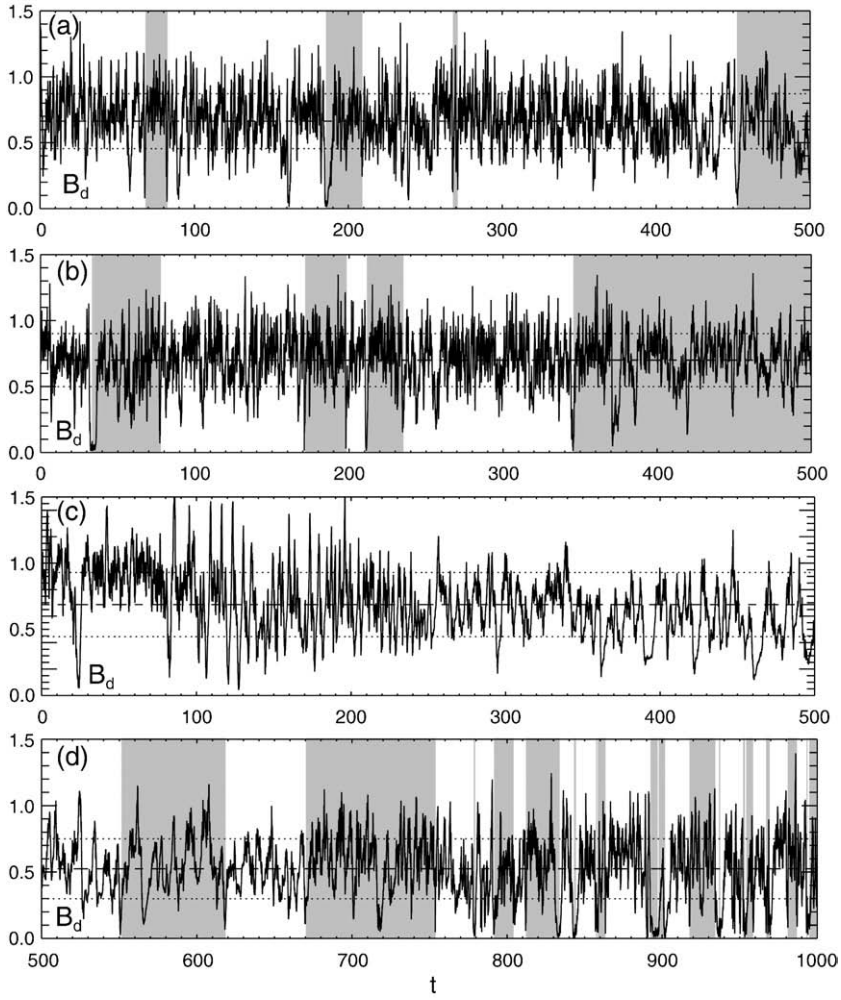

Fig. 1. Time series of rms dipole field intensity B_d on the outer core boundary, with the time average (dashed) and standard deviation (dotted) shown. From top to bottom: (a) regular evolution case R; (b) fixed parameter case R^*; (c) anomalous evolution case A, superchron portion; (d) anomalous evolution case A, reversing portion. Time t is in units of dipole free decay time t_d. Background shading indicates dipole polarity (grey is normal, white is reverse).

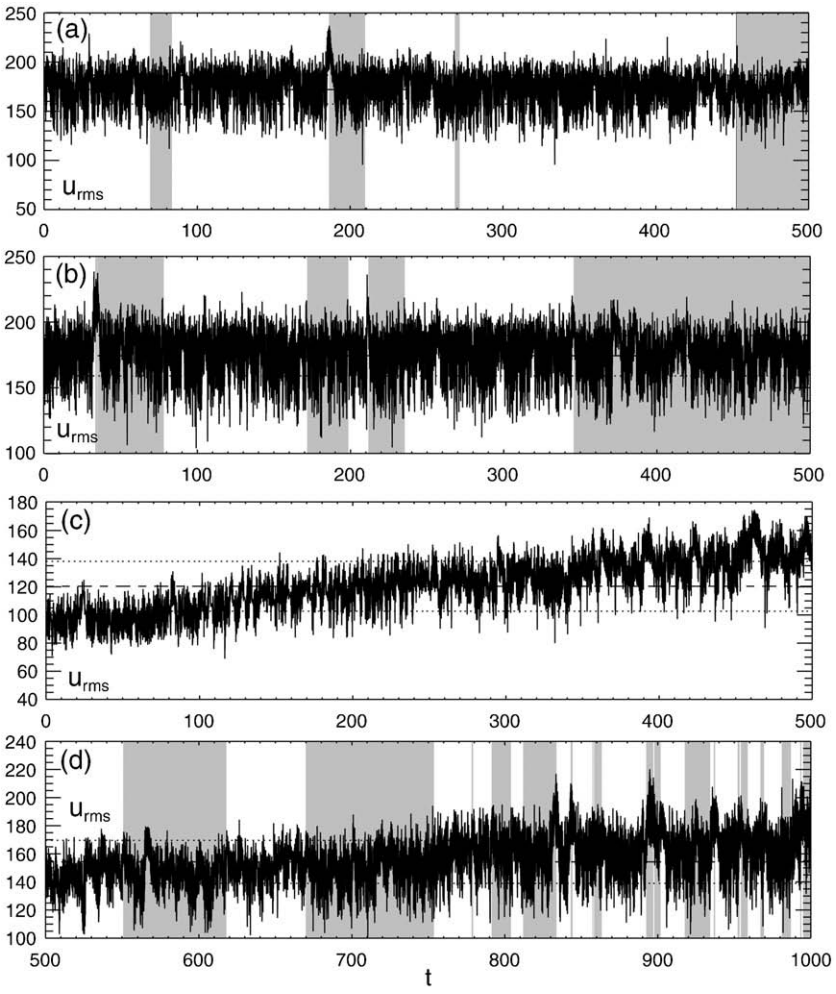

Fig. 2. Time series of rms fluid velocity $u_{\rm rms}$ in magnetic Reynolds number units, with the time average (dashed) and standard deviation (dotted) shown. From top to bottom: (a) regular evolution case *R*; (b) fixed parameter case R^*; (c) anomalous evolution case *A*, superchron portion; (d) anomalous evolution case *A* reversing portion. Time *t* is in units of dipole free decay time $t_{\rm d}$. Background shading indicates dipole polarity (grey is normal, white is reverse).

result in full polarity reversals. For cases *A* and A^* the dipole amplitude occasionally failed to recover following a collapse, and the dynamo remained stuck for a long time in a multi-polar state. This suggests that there exist some meta-stable transitional field configurations in this part of parameter space, possibly similar to the reversing dynamo state described by Nishikawa and Kusano (2008). These meta-stable states were encountered over limited ranges of the model evolution, usually in the regime where polarity reversals are present but widely separated in time. When these transitions occurred, we backed up and restarted the calculation at an earlier time with a small numerical truncation of the model variables. We found that these multi-polar transitions were generally not reproduced in the restarted simulation, although another such transition might occur later in the simulation. Because of these restarts, the parameter steps in case *A* are not of equal length. In contrast, the dipole collapse events were generally reproducible, and individual polarity reversals and dipole axis excursions were also reproducible. Just as significantly, there is no evidence of extremely strong magnetic field events. The maximum dipole field strength rarely exceeds $2\overline{B}_{\rm d}$ in any of the cases shown in Fig. 1. The absence of strong dipole events is a consequence of Lorentz force control on the convection. A very strong dipole field is not sustainable because the Lorentz force alters the flow and reduces its induction efficiency, causing the dipole field to decrease (Olson, 2007).

Important differences among these cases include the magnitudes of the long-term trends in some of the global variables. Table 2 shows that the secular trend in the internal field strength is less than the standard deviation of its fluctuations, i.e. $|\Delta B_{\rm rms}| < \sigma[B_{\rm rms}]$, in all cases. The same relationship is found for the fluid velocity except in the anomalous evolution case *A*. In case *R* and both fixed parameter cases, $|\Delta u_{\rm rms}|/\sigma[u_{\rm rms}] \le 0.3$, whereas in case *A* the secular trend in velocity is quite large compared to the fluctuations, with $\Delta u_{\rm rms}/\sigma[u_{\rm rms}] \simeq 3$. For the dipole field strength, $|\Delta B_{\rm d}|/\sigma[B_{\rm d}] \le 0.2$ for the two fixed cases, whereas $\Delta B_{\rm d}/\sigma[B_{\rm d}] = -0.43$ for case *R* and $\Delta B_{\rm d}/\sigma[B_{\rm d}] = -1.4$ for case *A*. Only in case *A* are the dipole and velocity trends larger than the standard deviation of their fluctuations, indicating a significant decrease in $\overline{B}_{\rm d}$ and increase in $\overline{u}_{\rm rms}$. The large trends in velocity and dipole field intensity in the anomalous evolution case *A* are clearly evident in Figs. 1 and 2. We consider a dynamo variable to be stationary if there is no significant trend in its mean value over time. According to our criterion, $B_{\rm d}$ and $u_{\rm rms}$ are stationary in the fixed parameter cases, marginally stationary in case *R*, and not stationary in case *A*.

Case *A* was deliberately constructed to simulate the transition from a non-reversing to a reversing dynamo, by starting with a low value of $\mathrm{Ra} = 1.69 \times 10^4$ (i.e., a slow rate of inner core growth) with a relatively strong, stable dipole and evolving to a larger value of $\mathrm{Ra} = 3.05 \times 10^4$ with a relatively weak, high variability dipole. The initial non-reversing (superchron) state persisted until the first reversal around

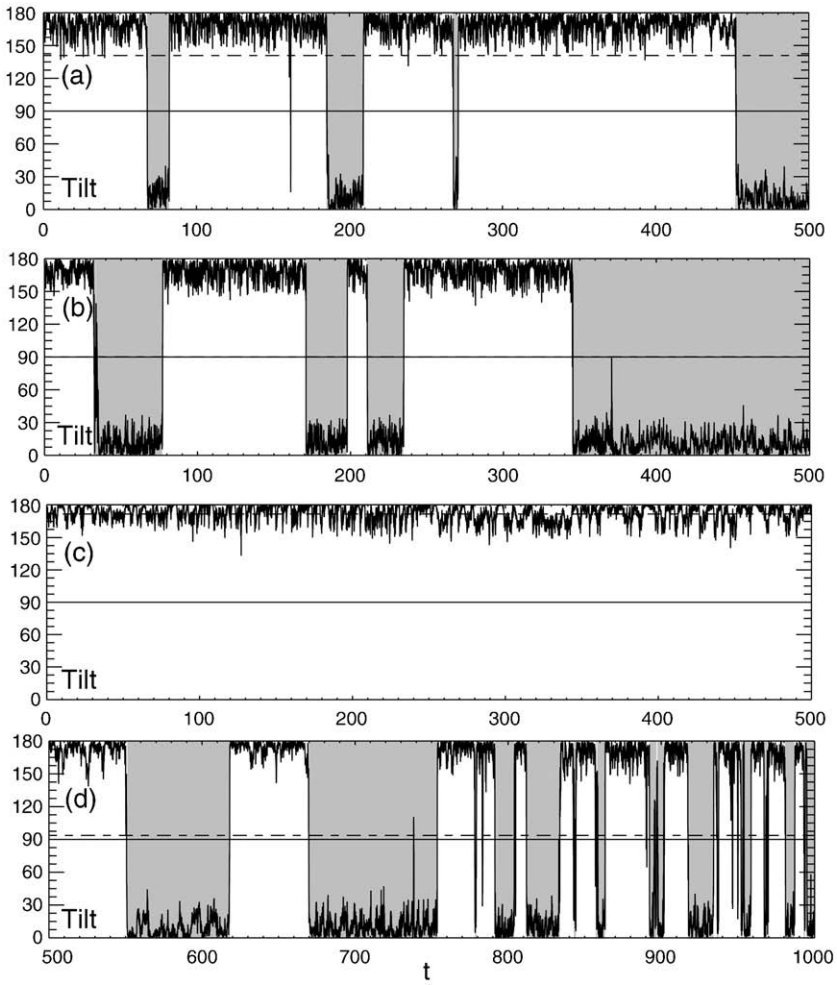

Fig. 3. Time series of dipole tilt in degrees, with the time average (dashed) shown. From top to bottom: (a) regular evolution case R; (b) fixed parameter case R^*; (c) anomalous evolution case A, superchron portion; (d) anomalous evolution case A reversing portion. Time t is in units of dipole free decay time t_d. Background shading indicates dipole polarity (grey is normal, white is reverse).

$t = 550$, equivalent to about 11 Myr of paleomagnetic time, at a value $\mathrm{Ra} = 2.51 \times 10^4$. The second part of the record includes some 26 polarity chrons plus several shorter excursion-type events, with a clear trend toward shorter chron length with time. The polarity bias b in Table 2 is defined in terms of a polarity function $p = \pm 1$, depending on the sign of the axial dipole. The polarity bias is $b = \overline{p} / \overline{|p|}$, the ratio of the mean polarity to its rms value, and is zero if the axial dipole spends an equal amount of time in normal and reversed polarity states. During the reversing part of case A ($t = 550$–1000) the polarity bias is nearly zero ($b = -0.03$), although the overall bias in this case is large ($b = -0.52$) by virtue of the long initial superchron.

4.2. Polarity statistics

The most dramatic evolutionary trends involve the polarity reversal statistics of case A, especially the length of the constant polarity chrons. All four cases include mixed length polarity chrons, but only case A shows evidence of systematic variations in their length (see Fig. 4). Cases R and R^* have essentially the same reversal frequency and number of major chrons (parts of 8 chrons in each case), although case R shows a substantial bias toward the polarity of its initial condition, whereas case R^* shows essentially zero polarity bias. In all four cases, simple polarity reversals account for about half of all the dipole axis equator crossings, denoted in Table 2 as N_{eq}, the total number of equator crossings. The remainder of these crossings are short-lived dipole excursions during stable chrons or are parts of complex reversals.

Fig. 4 summarizes the polarity statistics for the three cases, showing the polarity dispersion (i.e., chron length versus chron number), the correlation between the dipole intensity and the chron length, and histograms (pdfs) of the axial dipole field intensity. The axial dipole histograms all approximate symmetric bimodal distributions with finite overlap near zero, similar to statistical models of paleomagnetic secular variation (Constable and Parker, 1988). Suppression of the pdf tails occur at large intensities in every case, a consequence of the Lorentz force saturation discussed previously. Cases R and R^* are nearly symmetric about the two modes at $B_a \simeq \pm 0.7$. However, the pdf of case A shows evidence of some asymmetry about the modes and may conform to lognormal behavior at small intensities, the distribution predicted for multiplicative noise by Ryan and Sarson (2007).

To compare the distribution of these dipole intensities to normal and lognormal distributions we compute the Kolmogorov–Smirnov (K–S) statistic, which is a measure of the maximum deviation between two cumulative distributions (Press et al., 1992). According to the K–S statistic our dipole intensity distributions are consistent with randomly generated lognormal distributions only 0.1% of the time, and consistent with randomly generated normal distributions 0.01% of the time. Therefore, the dipole intensities may slightly favor lognormal behavior, but are

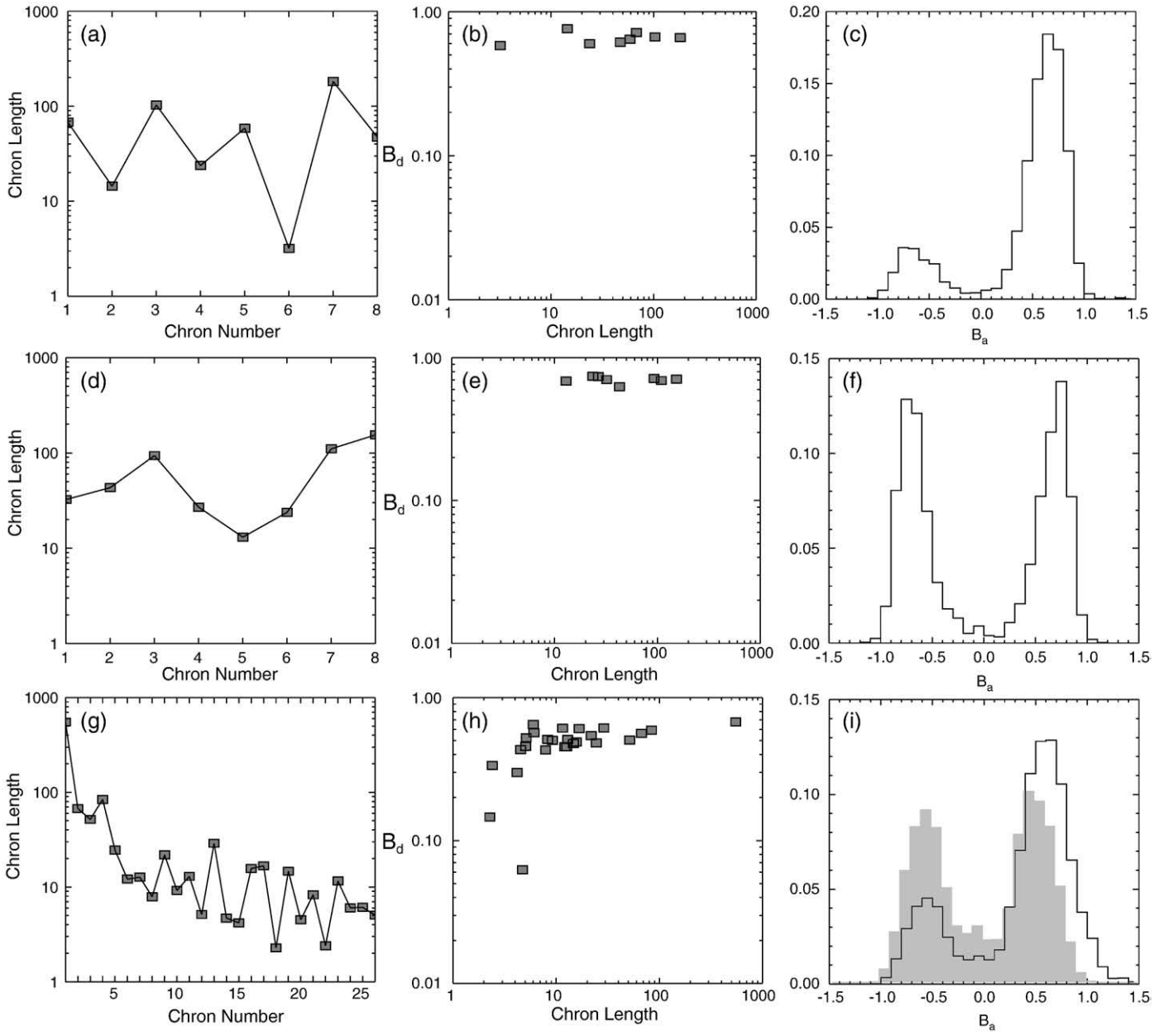

Fig. 4. Composite of dynamo model reversal statistics. Top row (a–c): dynamo case *R*; middle row (d–f): dynamo case R^*; bottom row (g–i): dynamo case *A*, with separate axial dipole pdfs shown for entire record (black line) and second half (gray filled). Left column: polarity chron length in dipole free decay time units versus chron number; center column: chron-averaged dipole intensity B_d versus chron length; right column: axial dipole B_a histogram (pdf).

not described well by either distribution. The K–S test is also applied to the chron lengths, and a measure of the significance of the K–S statistic, or *p*-value (Press et al., 1992), is reported. In the test for lognormality we find *p*-values of 0.94 for case *R*, 0.83 for case R^*, 0.49 for case *A*, and 0.95 for case A^*. A similar test for normality gives lower p-values of 0.81, 0.57, 10^{-4}, and 0.84 for those cases, respectively. Evidently, the presence of the superchron in case *A* makes the chron lengths appear much more like a lognormal than a normal distribution. Overall, our p-values are high compared to the *p*-value of 0.38 reported by Ryan and Sarson (2007) using a similar test on geomagnetic chron lengths going back to the CNS.

Cases *R* and R^* show some evidence of polarity dispersion, i.e., a statistical increase in polarity chron length with time, although the trend is quite small. In contrast, case *A* shows a marked polarity accumulation (inverse dispersion), equivalent to a statistical reduction in chron length with time. This trend is particularly strong with the initial superchron included, but is evident in the second half of the record as well. It is uncertain whether these statistical inferences are robust, however, due to the limited number of reversals in each record.

Some paleomagnetic studies indicate that average dipole intensity tends to be positively correlated with polarity chron length (see Constable, 2003; Valet et al., 2005). Fig. 4 shows this correlation for the three dynamos in this study. A positive dipole intensity-chron length correlation is evident in case *A* but negligible in cases *R* and R^*. Even in case A it is a relatively weak effect except for the shortest chrons, those lasting 5 dipole decay times (100 kyr) or less. Cases *R* and R^* show little evidence for this correlation, perhaps because they lack the short, low-intensity chrons found in case *A*.

4.3. Frequency spectra

Fig. 5 shows frequency spectra of rms internal magnetic field B_{rms}, rms dipole B_d and axial dipole fields B_a on the core boundary, and rms velocity u_{rms} for the four cases. The first row shows cases R (black) and R^* (red), the second row shows the first half of case A (black) and all of case A^* (red), and the third row shows the second half of case A (black) and all of case A^* (red). Frequency is scaled by $1/t_d$, and variance-preserving Hanning tapers with 21-point smoothing filters were applied in calculating these spectra. Reference power-law slopes have been added for comparison purposes.

Like the geomagnetic power spectrum (see Constable and Johnson, 2005), these spectra are broad-band and dominated by low frequency energy. Evidence of wave energy concentrated at discrete frequencies is conspicuously lacking. Even though the variance decreases more-or-less continuously over nearly 5 decades of frequency, the magnetic field and velocity spectra both show evidence of distinct frequency regimes. An elevated ultra-low frequency plateau with a knee around $f=0.01$ is particularly well-developed in the superchron portion of evolving case A, but is also seen in the spectra of case R. Fixed case A^* has an ultra-low frequency plateau, but it is not elevated and it lacks the knee structure connecting it to the rest of the spectrum. The elevation of the ultra-low frequency plateau is primarily due to the secular trends in magnetic field intensity and fluid velocity in the evolving cases, although the dispersion of polarity chron lengths also makes a contribution to this structure. Specifically, we find that the ultra-low frequency plateaus are attributable to the secular trends in case R^* (in the B_{rms}, B_d and u_{rms} -spectra), case R (in the B_{rms}, and B_d -spectra), the first half of case A (in the B_d and u_{rms} -spectra), and the second half of case A (in the B_{rms}, B_d and u_{rms}-spectra). For these spectra the low frequency plateaus are absent when the secular trend is removed. The exception is the low frequency plateau of the axial

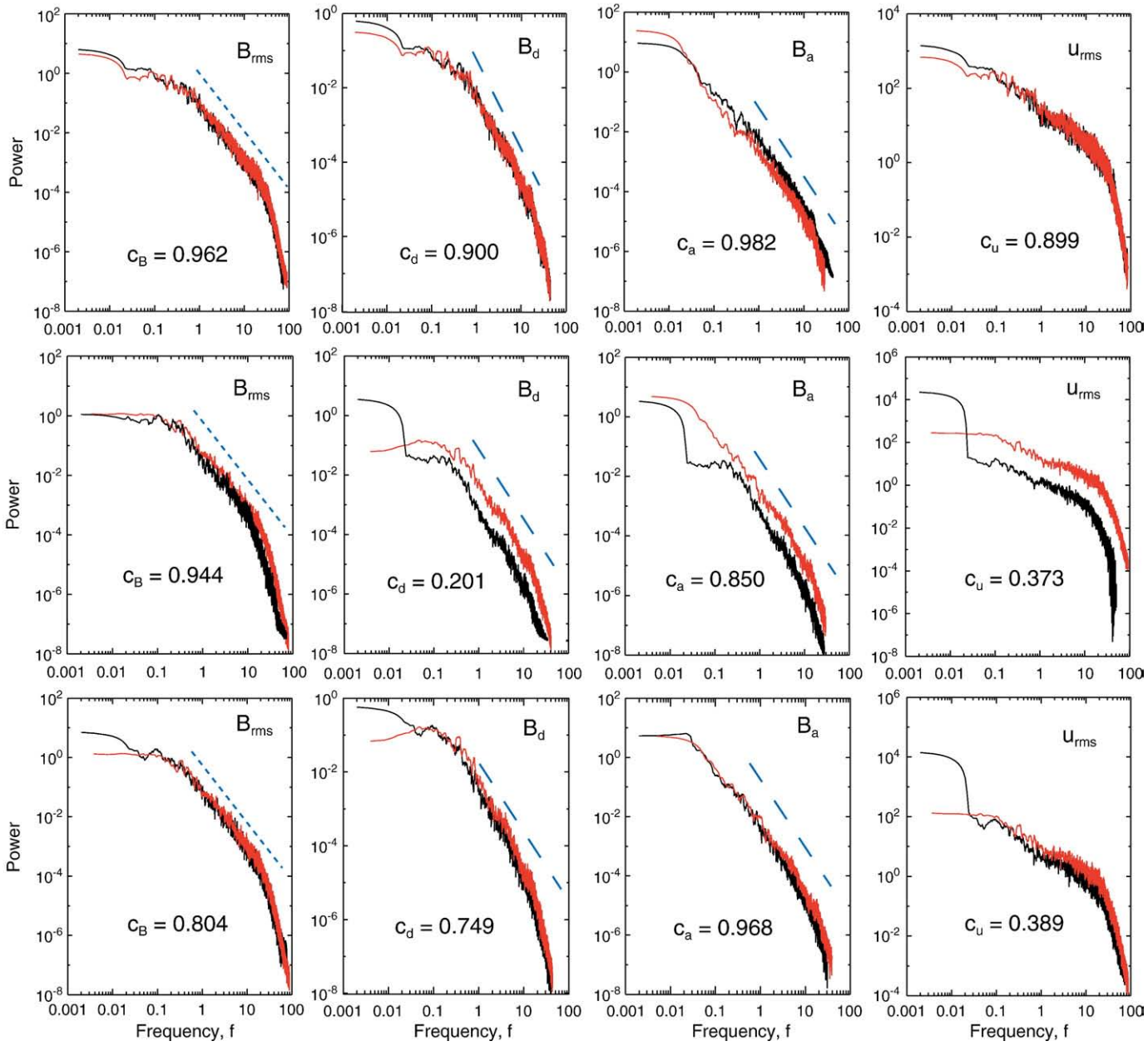

Fig. 5. Composite of dynamo model frequency spectra scaled by dipole free decay time. Columns from left to right: rms internal magnetic intensity B_{rms}; rms core boundary dipole intensity B_d; rms core boundary axial dipole intensity B_a; rms fluid velocity u_{rms}. Top row: dynamo cases R (black) and R^* (red); Middle row: dynamo case A first half (black) and all of A^* (red). Bottom row: dynamo case A second half (black) and all of A^* (red). Reference power-law slopes are $n=-2$ (dotted) and $n=-7/3$ (dashed). Correlation coefficients c are shown for each pair of spectra.

dipole B_a, which we find is not due to the secular trend in any of these cases and is likely attributable to the sign changes of B_a.

In the low frequency band, that is $0.1<f<10$, power-law (f^n-type) behavior is seen in all the spectra, with exponents near $n=-2$ (dotted line) for the internal magnetic field and near $n=-7/3$ (dashed line) for the dipole and the axial dipole fields on the core boundary. The fluid velocity spectra also have approximate power-law behavior in this band, but with smaller slopes. The internal magnetic field and velocity spectra include an additional knee structure near $f\simeq 20$, and all the spectra have very steep slopes in the high frequency band, $f>20$. Also shown in Fig. 5 are the correlation coefficients c between each pair of spectra. Cases R and R^* are correlated with $c\geq 0.899$, confirming that they have similar time variability. The differences between cases A and A^* are most evident in the first half of B_d and both u_{rms} -spectra, where the correlations are all less than 0.4, and are attributable to the large secular trends of case A.

5. Discussion and geomagnetic implications

One of the main goals in modeling the evolution of the geodynamo is to simulate the ultra-long time-scale changes in reversal frequency, including the approximately 200 Myr between superchrons (Pavlov and Gallet, 2005). By compressing these very long time scales we are able to simulate geomagnetic evolution, but at the cost of some realism. The evolution employed in this study has at least three simplifications. First, our simulation times, 20 Myr (case A) and 10 Myr (case R), are too short to provide robust reversal statistics. Second, because our model parameters Ra and E change more than 10 times faster than expected for core evolution over the past 100 Myr (see Section 2) subtle evolutionary effects in the geodynamo may be missing from our model. Third, our model parameters are evolved in steps instead of continuously, with the possible consequence that our reversal time scales are close to the evolution time scales, making it difficult to separate stochastic reversal behavior from reversal rate changes due to evolution. Longer runs with slower evolution would better separate these time-scales.

In spite of these limitations, our calculations reveal some testable signatures of geodynamo evolution. In comparison with the fixed-parameter dynamo simulations, evolving case A predicts an observable increase in reversal frequency and decrease in dipole strength with increasing Ra. Similarly, increasing E has an observable effect on reversal frequency and dipole strength. In the regular evolution case R, the expected decrease in reversal frequency due to decreasing Ra is compensated by the effects of decreasing angular velocity of rotation (increasing E), so that polarity dispersion and secular trends in magnetic field strength and convective velocity are reduced. In this respect the reversal statistics of the regular evolution and fixed case, R and R^*, are almost identical, with a low but non-zero reversal frequency. This implies that the evolutionary vector as described in Section 2 is nearly parallel to a dynamo regime boundary. For the fixed $E=6.5\times10^{-3}$ value of case A, regular evolution predicts reversals should be present at $Ra=2.75\times10^4$, which is larger than the value of $\mathrm{Ra}=2.51\times10^4$ where the superchron ends. This would imply that there was no substantial delay of the first reversal coming out of the superchron (i.e. no hysteresis) for case A, although this may be model dependent behavior.

According to our results, if the geodynamo resides near a reversing-nonreversing boundary in parameter space, then a transient episode of anomalous evolution could be responsible for the termination (or similarly the initiation) of a superchron. Regular monotonic core evolution as predicted by thermal history models, coupled with tidal deceleration tends to produce slower (possibly negligible) evolution, which may account for the rather steady average geomagnetic dipole moment over last several hundred million years (Tauxe and Yamazaki, 2007). Multiple superchrons in the paleomagnetic record suggest that either there have been perturbations to regular evolution, such as an episode of anomalous inner core growth, or that the geodynamo has undergone regular evolution across a non-monotonic (rough) reversal regime boundary (Driscoll and Olson, 2007). Case R shows nearly constant reversal statistics, implying that the regime boundary is rather monotonic along this path in Ra–E space, and that an episode of anomalous evolution is the favored mechanism to initiate a superchron. Although superchrons can be described as stochastic events in a complex system, such as the geodynamo (Ryan and Sarson, 2007), the polarity chron dispersion of the geodynamo over the last 100 Myr (Gallet and Courtillot, 1995) is strong evidence for anomalous core evolution, as shown by our anomalous evolution model.

Comparison of these models with paleomagnetic field behavior can also be made in the frequency domain. The composite geomagnetic dipole spectrum of Constable and Johnson (2005) includes an elevated ultra-low frequency plateau that is separated from the rest of the spectrum by a knee structure at a frequency of about $f=0.2$ Myr^{-1} ($0.004\ t_d^{-1}$), which they interpret as the boundary between superchron and reversing geodynamo regimes. The comparable knee-structures in Fig. 5 occur at frequencies near $f=0.5$ Myr^{-1} ($0.001\ t_d^{-1}$), assuming $t_d=20$ kyr for the dipole free decay time. We attribute the difference in knee frequencies to the accelerated rate of evolution in our dynamo models compared to the actual rate of core evolution. Constable and Johnson (2005) identify an additional knee feature at intermediate frequency, about $f=20$ Myr^{-1} ($0.04\ t_d^{-1}$), which is prominent in the dipole spectrum of the superchron portion of case A. At intermediate frequencies, the slope of the dynamo model magnetic spectra are in the range f^{-2}–$f^{-7/3}$, with still larger slopes at higher frequencies, again similar to the observed geomagnetic spectrum in this range (Courtillot and Le Moul, 1988).

Several properties of geodynamo evolution that are not considered here include the conductivity and size of the inner core, and the pattern of heat flux at the CMB. It has been proposed that the electrically conductive inner core (with a dipole decay time of about 3 kyr) can influence the frequency of dipole field reversals in the outer core (Hollerbach and Jones, 1993; Gubbins, 1999). A comparison of dynamo models with a conducting and an insulating inner core by Wicht (2002) found this effect to be significant only in frequently reversing models, with typical chron lengths of 10 kyr or less. The models presented here with an insulating inner core reverse on a much longer time-scale, with typical chron lengths of 100 kyr–1 Myr. Therefore, we expect that the behavior of the numerical models presented here regarding the long-time scale evolution of the geodynamo will not be sensitive to the conductivity of the inner core, although we acknowledge this may be an important effect in the Earth's core.

The influence of the size of the inner core on the geodynamo has been explored in several previous studies, but the results are not definitive. Sakuraba and Kono (1999) find that the presence of an inner core has a stabilizing effect on the dipole field. Heimpel et al. (2005) find qualitatively similar results, that the dipole strength increases with increasing inner core size, up to about half of the outer core radius. According to their results we would expect an increase in B_d of only about 2% solely due to an increase in inner core size of 83 km (Table 1). Roberts and Glatzmaier (2001) compare three models: a past model with a small inner core radius ($r_i/4$), a generic model with the present-day inner core radius ($r_i=1221$ km), and a future model with a large inner core radius ($2r_i$). They find a stronger and more stable dipole field with the smallest inner core, in contrast to Heimpel et al. (2005). However, Roberts and Glatzmaier (2001) actually test more than just the effect of inner core size, because they also vary the core heat flow and the rotation rate. In our notation, the parameter differences between their models correspond to $\Delta Ra/\overline{Ra}=-160\%$ and $\Delta E/\overline{E}=+85\%$ (where overbar denotes the mean value) for their small versus generic inner cores, and $\Delta Ra/\overline{Ra}=-175\%$ and $\Delta E/\overline{E}=+160\%$ for their generic versus large inner cores. In going from the past to the future, Roberts and Glatzmaier (2001) also reduce the influence of rotation which would tend to make the dipole less stable with time according to our results.

Dynamo models indicate that the stability of the dipole field is also sensitive to the pattern of heat flux variations on the CMB. Glatzmaier et al. (1999) examined reversal behavior in dynamos with a variety of CMB heat flux patterns. Their calculations showed that certain boundary heat flow patterns produce more frequent reversals than others. Although the exact relationship between reversal rate and boundary heterogeneity does not appear to be simple, they found that a dynamo with uniform heat flux at the CMB is most 'Earth-like' in terms of its reversal behavior. Accordingly, paleomagnetic reversal frequencies may reflect a combination of changes in CMB heterogeneity, decreases in the rate of rotation, and thermo–chemical core evolution.

In numerical dynamos with both homogeneous and heterogeneous CMB conditions, the stability of the dipole field is found to correlate with the amount of equatorial antisymmetry of the entire field (Coe and Glatzmaier, 2006; Takahashi et al., 2007; Olson et al., 2009). This suggests that the gross asymmetry of the geomagnetic field could be attributed to the interplay between boundary heterogeneity, rotation, and thermo–chemical evolution. Future evolutionary dynamo modeling should examine the relative importance of all three.

There are numerous ways to improve the evolving geodynamo models presented here, including continuous parameter evolution constrained by a full thermal history model of the core in conjunction with a more detailed rotational history, continuous growth of the inner core which would likely require adaptive re-meshing of the numerical grid, core-mantle boundary condition evolution, coupled thermal–chemical (i.e., co-density) evolution, and longer simulation times.

Acknowledgments

We would like to thank S. Stanley and an anonymous reviewer for their helpful comments. We gratefully acknowledge the support through grant EAR-0604974 from the Geophysics Program of the National Science Foundation.

References

Aubert, J., Aurnou, J., Wicht, J., 2008. The magnetic structure of convection-driven numerical dynamos. Geophys. J. Int. 172, 945–956.
Berhanu, M., et al., 2007. Magnetic field reversals in an experimental turbulent dynamo. EPL 77, 59001.
Buffett, B.A., 2003. The thermal state of the Earth's core. Science 299, 1675–1676.
Butler, S.L., Peltier, W.R., Costin, S.O., 2005. Numerical models of the Earth's thermal history: effects of inner-core solidification and core potassium. Phys. Earth Planet. Int. 152, 22–42.
Coe, R., Glatzmaier, G., 2006. Symmetry and stability of the geomagnetic field. Geophys. Res. Lett. 33.
Constable, C.G., 2000. On the rates of occurence of geomagnetic reversals. Phys. Earth Planet Int. 118, 181–193.
Constable, C.G., 2003. Geomagnetic reversals: rates, time scales, preferred paths, statistical models and simulations. In: Jones, C.A., Soward, A.M., Zhang, K. (Eds.), Earth's core and lower mantle. Taylor and Francis, London, pp. 77–99.
Constable, C.G., Parker, R.L., 1988. Statistics of geomagnetic secular variation for the past 5 m.y. J. Geophys. Res. 93, 11569–11581.
Constable, C.G., Johnson, C., 2005. A paleomagnetic power spectrum. Phys. Earth Planet. Int. 153, 61–73.
Courtillot, V., Le Moul, J.L., 1988. Time variations of the Earth's magnetic field: from daily to secular. Ann. Rev. Earth Planet. Sci. 16, 389–476.
Courtillot, V., Olson, P., 2007. Mantle plumes link magnetic superchrons to Phanerozoic mass depletion events. Earth Planet. Sci. Lett. 260, 495–504.
Christensen, U.R., Wicht, J., 2007. Numerical dynamo simulations. In: Olson, P. (Ed.), Treatise on Geophysics, vol. 8. Elsevier B.V., pp. 245–282.
Driscoll, P., Olson, P., 2007. Polarity reversal statistics in geodynamo simulations. AGU, Fall Meeting 2007, GP33A-0920.
Dziewonski, A., Anderson, D., 1981. Preliminary reference Earth model. Phys. Earth Planet. Inter. 25.
Gallet, Y., Courtillot, V., 1995. Geomagnetic reversal behaviour since 100 Ma. Phys. Earth Planet. Inter. 92, 235–244.
Glatzmaier, G.A., Coe, R.S., 2007. Magnetic reversals in the core. In: Olson, P. (Ed.), Treatise on Geophysics, vol. 8. Elsevier B.V., pp. 283–299.
Glatzmaier, G.A., Coe, R.S., Hongre, L., Roberts, P.H., 1999. The role of the mantle in controlling the frequency of geomagnetic reversals. Nature 401, 885–890.
Gubbins, D., 1999. The distinction between geomagnetic excursions and reversals. Geophys. J. Int. 137, 14.
Gubbins, D., Alfe, D., Masters, G., Price, G., Gillan, M., 2003. Can the Earth's dynamo run on heat alone? Geophys. J. Int. 155, 609–622.
Gubbins, D., Alfe, D., Masters, G., Price, G., Gillan, M., 2004. Gross thermodynamics of two-component core convection. Geophys. J. Int. 157, 1407–1414.
Heimpel, M.H., Aurnou, J.M., Al-Shamali, F.M., Gomez Perez, N., 2005. A numerical study of dynamo action as a function of spherical shell geometry. Earth Planet. Sci. Lett. 236, 542–557.
Heller, R., Merrill, R.T., McFadden, P.L., 2002. The variation of intensity of Earth's magnetic field with time. Phys. Earth Planet. Int. 131, 237–249.
Hollerbach, R., Jones, C., 1993. Influence of the Earth's inner core on geomagnetic fluctuations and reversals. Nature 365, 541–543.
Hoyng, P., Ossendrijver, M., Schmidt, D., 2001. The geodynamo a a bistable oscillator. Geophys. Astrophys. Fluid Dyn. 94, 263–314.
Hulot, G., Gallet, Y., 2003. Do superchrons occur without any paleomagnetic warning? Earth Planet Sci. Lett. 210, 191–201.
Jones, C.A., 2007. Thermal and compositional convection in the outer core. In: Olson, P. (Ed.), Treatise on Geophysics, vol. 8. Elsevier B.V., pp. 131–176.
Jonkers, A.R.T., 2003. Long-range dependence in the Cenozoic reversal record. Phys. Earth Planet. Int. 135, 253–266.
Kageyama, A., Miyagoshi, T., Sato, T., 2008. Formation of current coils in geodynamo simulations. Nature 454, 1106–1109. doi:10.1038/nature07227.
Kutzner, C., Christensen, U.R., 2000. Effects of driving mechanisms in geodynamo models. Geophys. Res. Lett. 27, 29–32.
Kutzner, C., Christensen, U.R., 2002. From stable dipolar to reversing numerical dynamos. Phys. Earth Planet. Int. 131, 29–45.
Labrosse, S., 2003. Thermal and magnetic evolution of the Earth's core. Phys. Earth Planet. Int. 140, 127–143.
Lambeck, K., 1980. The Earth's Variable Rotation: Geophysical Causes and Consequences. Cambridge University Press.
Loper, D.E., 2007. Turbulence and small-scale dynamics of the core. In: Olson, P. (Ed.), Treatise on Geophysics, vol. 8. Elsevier B.V., pp. 187–206.
Merrill, R.T., McFadden, P.L., 1999. Geomagnetic polarity transitions. Rev. Geophys. 37, 201–226.
Nimmo, F., 2007. Energetics of the core. In: Olson, P. (Ed.), Treatise on Geophysics, vol. 8. Elsevier B.V., pp. 31–65.
Nimmo, F., Price, G.D., Brodholt, J., Gubbins, D., 2004. The influence of potassium on core and geodynamo evolution. Geophys. J. Int. 156, 363–376.
Nishikawa, N., Kusano, K., 2008. Simulation study of the symmetry-breaking instability and the dipole field reversal in a rotating spherical shell dynamo. Phys. Plasmas 15, 082903.
Olson, P., 2007. Gravitational dynamos and the low frequency geomagnetic secular variation. Proc. Natl. Acad. Sci. 104, 20159–20166.
Olson, P., Driscoll, P., Amit, H., 2009. Dipole collapse and reversal precursors in a numerical dynamo. Phys. Earth Planet. Int 173, 121–140.
Pavlov, V., Gallet, Y., 2005. A third superchron during the early Paleozoic. Episodes 28, 78–84.
Press, W., Teukolsky, S., Vetterling, W., Flannery, B., 1992. Numerical Recipes in C: The Art of Scientific Computing, 2nd edition. Cambridge Univ. Press, New York.
Roberts, P., Glatzmaier, G., 2001. The geodynamo, past, present and future. Geophys. Astrophys. Fluid Dyn. 94, 47–84.
Ryan, D.A., Sarson, G.R., 2007. Are geomagnetic field reversals controlled by turbulence with the Earth's core? Geophys. Res. Lett. 34, L02307–12.
Sakuraba, A., Kono, M., 1999. Effect of the inner core on the numerical solution of the magnetohydrodynamic dynamo. Phys. Earth Planet. Int. 111.
Stacy, F.D., 1992. Physics of the Earth. Brookfield Press, Brisbane, Australia.
Takahashi, F., Matsushima, M., Honkura, Y., 2007. A numerical study on magnetic polarity transition in an MHD dynamo model. Earth Planets Space 59, 665–673.
Takahashi, F., Matsushima, M., Honkura, Y., 2008. Scale variability in convection-driven MHD dynamos at low Ekman number. Phys. Earth Planet. Int. 132, 168–178.
Tauxe, L., Yamazaki, T., 2007. Paleointensities. In: Kono, M. (Ed.), Treatise on Geophysics, vol. 5. Elsevier B.V., pp. 509–563.
Terasaki, H., Suzuki, A., Ohtani, E., Nishida, K., Sakamaki, T., Funakoshi, K., 2006. Effect of pressure on the viscosity of Fe-S and Fe-C liquids up to 16 GPa. Geophys. Res. Lett. 33, 22307.
Valet, J.P., 2003. Time variations in geomagnetic intensity. Rev. Geophys. 41 (1), 1004. doi:10.1029/2001RG000104.
Valet, J.P., Meynadier, L., Guyodo, Y., 2005. Geomagnetic dipole strength and reversal rate over the past two million years. Nature 435, 802–805.
Wicht, J., 2002. Inner-core conductivity in numerical dynamo simulations. Phys. Earth Planet. Inter. 132, 281–302.
Wicht, J., 2005. Palaeomagnetic interpretation of dynamo simulations. Geophys. J. Int. 162, 371–380.
Wicht, J., Stellmach, S., Harder, H., 2009. Numerical models of the geodynamo: from fundamental cartesian models to 3D simulations of field reversals. Geomagnetic Field Variations. Springer, p. 107.
Wood, B., Walter, M., Wade, J., 2006. Accretion of the earth and segregation of its core. Nature 441, 825.
Zharkov, V.N., Molodensky, S.M., Brzezinski, A., Groten, E., Varga, P., 1996. The Earth and its Rotation: Low Frequency Geodynamics. Wichmann, Heidelberg.
Zhenyu, Z., Yaoqi, Z., Guosheng, J., 2007. The periodic growth increments of biological shells and the orbital parameters of the Earth–Moon system. Environ. Geol. 51, 1271–1277.